12

Numerical Modeling and Calculation of Sensing Parameters of DNA Sensors

Hediyeh Karimi[1], Farzaneh Sabbagh[2], Mohammad Eslami[3], Hamid sheikhveisi [4], Hossein Samadyar [5] and Omid Talaee[6]

[1]Malaysia Japan International Ins. of Technology, Universiti Teknologi Malaysia, Kuala Lumpur, Malaysia
[2]Department of Bioprocess Engineering, Faculty of Chemical Engineering, University Technology Malaysia, Johor, Malaysia
3Department of Electrical & Computer, College of Engineering, Islamic Azad University, Zahedan Branch, Zahedan, Iran
4Department Of Computer Engineering, Payame Noor University, IR. Iran
5Young Researchers and Elites club, Science and Research Branch, Islamic Azad University, Tehran, Iran
6Department of Nuclear and Heat Power Engineering, Faculty of Energy and Transport System, Peter the Great Saint-Petersburg Polytechnic University, Saint-Petersburg, Russia

Abstract

These days, construction and operation of label-free DNA biosensors are the definitive factors for achieving trustworthy laboratory tests. Hence, detection systems or sensors using new emerging nanomaterials are considered as powerful tools for the genetic researchers to understand the progression and early screening of diseases, routine walk-in medical checkups, which make the controlled design of these sensors vital. Nanotechnology has devoted itself for the purpose of producing very sensitive and reliable biosensors. Despite these efforts, the sensing mechanism in label-free field-effect-based DNA sensors has aroused a great deal of controversy among scientists. In order to find an answer for these questions, developing the analytical model of these sensors expected to help. In addition, just computational calculations can allow designers to evaluate the importance of several parameters involved in the fabrication and provide a framework to which experimental results can be compared. In this chapter, we present a numerical model for the current–voltage characteristic of graphene-based liquid-gated field effect transistors (FETs), which include the calculation of the conductance changes in the sensor's response during DNA hybridization. The results are compared with the experimental work and an acceptable agreement is observed.

*Corresponding author: h.karimifeizabadi.2013@ieee.org

Ashutosh Tiwari, Hirak K. Patra and Anthony P.F. Turner (eds.) Advanced Bioelectronic Materials, (429–452) © 2015 Scrivener Publishing LLC

Keywords:

12.1 Introduction to Graphene

The nanomaterials of graphene (sp^2 aromatic)-based carbon have been widely used for biosensing, and they have been the subject of much interest, even though it has been a relatively short period since discovery of them. Graphene and its derivatives such as the graphene oxide (GO), reduced graphene oxide (rGO), and n-doped graphene are reported to be used successfully in biosensing applications [1]. An oxidized form of graphene, GO, created in solution with highly negative charges and hydrophilicity characteristic has been used as a template for DNA hybridization studies [2]. The fabrication process of GO has a strong influence on the electrical possessions of GO films which have been employed in sensor configuration. On the other hand, the sensitivity of these sensors produced from GO are dependent on some factors such as size, shape, presence of wrinkles, defects, and oxidation degree of GO sheets. Therefore, from the point of fabrication, more studies and supervision are required to control the quality of fabrication of GO sheets [3–5]. In contradiction of GO, large-size graphene layers are claimed as more reliable and beneficial nanomaterials in biosensing experiments from the device fabrication viewpoint.

Graphene provides a two-dimensional (2D) honeycomb structure consisting of a thin layer of single carbon atoms. The reason for that being the idiosyncratic physical and chemical characteristics like exceptional strength [6], and its great thermal conductivity plus biocompatibility that it possess [7]. Graphene, as a nearly perfect 2D crystal free of the structural defects [8–9], presents surprisingly ballistic transport due to its significant high electron mobility at low temperatures that can reach up to 200 000 cm^2/Vs with typical carrier concentration of 2×10^{11} cm^{-2} [10, 11]. Graphene and nanotubes have been utilized as an essential element in several electronic devices, e.g., biosensors [12, 13]. There has been major evidence indicating biosensing applications shown in graphene and its by-products [14]. Due to the biocompatibility and extreme environmental distress affectability of thin graphene plates, it provides an essential biosensing application for them. Meaning that they are greatly sensitive to variables such as electronic doping [15–18] and molecule adsorption [3,14,19–20]. In addition, it is considerable that, because of easier contact, the surface structure of graphene (displayed in Figure 12.1) in comparison

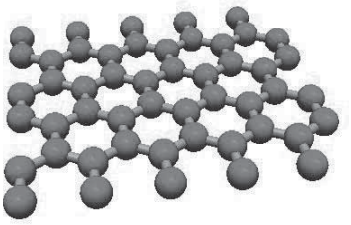

Figure 12.1 Schematic of graphene as a sensing layer.

to other carbon derivatives ensures a higher adsorption of DNA molecules [21]. This resulted in the selection of graphene as the DNA detection sensory framework in this study.

12.1.1 Electronic Structure of Graphene

Understanding the electronic structure of graphene is the starting point for pursuing the electronic properties of graphene. Intrinsic graphene is known as a semimetal with zero bandgap [22]. It is widely claimed that its valence and conduction bands are cone shaped and meet at the K points of the Brillouin zone [22, 23]. Because the bandgap is zero, devices with channels made of large-area graphene cannot be switched off and therefore are not suitable for logic applications. However, bandgap can be induced in these materials with two demonstrated ways [22]. Firstly, narrowing the graphene to nanoribbon, by which its bandgap has a reverse relation with the width of nanoribbon in this method [24]. Secondly, by applying a perpendicular electric field to bilayer graphene (BLG) that results a potential difference between layers which opens the bandgap in BLG [25, 26]. Although the physical simulation is accurate enough, there are still many controversies about their ability to compute the potential model of the device. Analytical modeling possibly will facilitate this challenge. But, it needs serious improvement due to the lack of effective mass effect on the vertical electric field proposed by Ref. [27].

12.1.2 Graphene as a Sensing Element

Maximum surface-to-volume ratio for sensing application would be provided by employing graphene with its unique 2D structure, exposing every atom of graphene to the environment. Furthermore, graphene shows no distinction between surface sites and the bulk material, which is the major motivation behind implementation of other nanostructured materials. Exceptional electronic structure and interesting properties of graphene

resulted in the adaptability of graphene as a basic sensing element in sensor application. The ambipolarity can be mentioned as one of the important characteristic of graphene, meaning that "chemical gating" of the material can be achieved by adsorption of either electron withdrawing or donating groups, which can be easily monitored in a resistive-type sensor setup. In other words, a graphene-based field effect transistor (FET) is an ambipolar device. It can operate via both electron and hole branches where the conductivity changes as a function of the electron or hole concentration and is proportional to the gate voltage [28]. Any molecular disruption on the graphene can be easily detected due to its ultrahigh surface area combing with its specific electronic features. Our expectations from graphene-oriented sensors for detection of individual molecules on and off its surface have become high because of its unique structures. The availability of 2D graphene will open up possibilities for designing and preparing graphene-oriented electrodes for a wide range of liquid-sensing and biosensing applications ranging from amperometric sensors to amperometric enzyme biosensors and label-free DNA biosensors. With the help of the study and molecular analysis of nucleic acids, almost 400 and increasing genetic conditions are diagnosable now [29].

12.1.3 DNA Molecules

A diagram of the DNA molecule is drawn in Figure 12.2 [30], where it is shown that the DNA molecule is a polyelectrolyte comprised of two helically wound sugar–phosphate backbones, joined in the middle by nucleobases (adenine, thymine, cytosine, and guanine). The strong hydrogen bonds between matching nucleobases keep the two strands together (AT and CG), as well as with dispersion forces that occur between the stacked flat nucleobases [31]. The phosphate groups are negatively charged in biologically relevant conditions (25°C, 1 mM–1 M monovalent salt concentration, pH 7). It is strongly believed that the signal changes in a BioFET would occur because of the negative charges of phosphate groups either directly or indirectly, as DNA molecules attached to the surface [32].

12.1.4 DNA Hybridization

The process of establishing a non-covalent, sequence-specific interaction between two or more complementary strands of nucleic acids into a single complex is known as a hybridization phenomenon which in the case of the two strands is referred to as a duplex. The detection of DNA hybridization has been a topic of central importance owing to a wide variety of

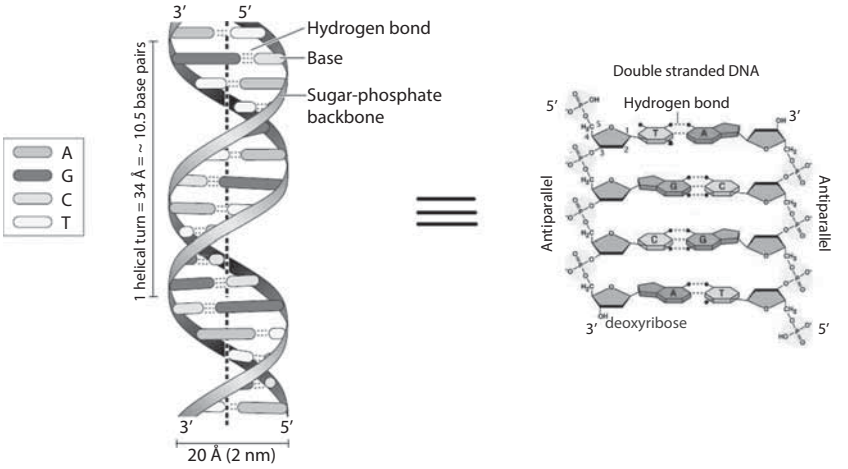

Figure 12.2 Helical and detailed structure of DNA molecules.

applications such as diagnosis of pathogenic and genetic disease, gene expression analysis, and the genotyping of mutations and polymorphisms [33, 34]. Technologies in DNA biosensing [35] have received special appeal not only for their low cost and simplicity, but for their ultimate capabilities in detecting single-nucleotide polymorphisms (SNP) which have been correlated to several diseases and genetic disorders such as Alzheimer's and Parkinson's diseases.

The DNA hybridization event is the basis of many existing DNA detection techniques. In DNA hybridization as depicted in Figure 12.3, the target, unknown single-stranded DNA (ssDNA), is identified and formed by a probe ssDNA and a double-stranded (dsDNA) helix structure with two complementary strands. It is believed that, in the presence of a mixture of diverse non-complementary nucleic acids, the hybridization reaction is known to be extremely efficient and specific. The basis for the high specificity of the biorecognition process is the uniqueness of the complementary nature of this binding reaction between the base pairs, i.e., adenine–thymine and cytosine–guanine.

In a graphene-based FETs (GFETs) with DNA application, the DNA molecules used as probes are short (typically 20–30 bases long). ssDNA probes could be captured on a surface through long-range electrostatic forces or by chemical combination with an activated (or functionalized) surface. The success of a DNA sensor depends on the high specificity of capturing only the exact complementary target, allowing DNA sensors to detect SNP. For this purpose, the DNA probes should be made short such

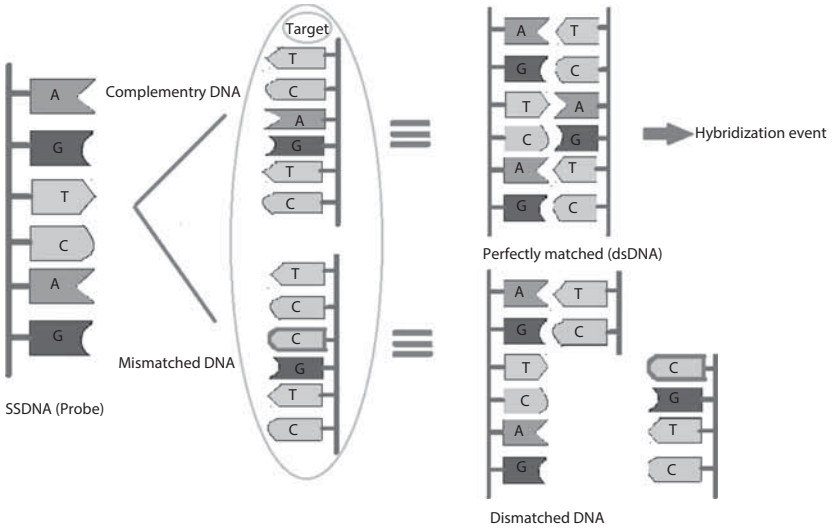

Figure 12.3 Schematic of DNA hybridization event.

that the energy of binding is severely changed with a single mismatch, prohibiting nonspecific pairing. Therefore, faster and more precise hybridization rate would obtained by choosing the shorter probes (oligonucleotides). It is noteworthy that the density of capture probes should be high to avoid targets absorbing and attaching to vacant sites on the surface. Also, there is another way to deactivate the vacant sites by a chemical step, but such processes are not perfect, and active sites can still exist.

The hybridization experiment should be carried out in a buffer solution with precisely selected ionic concentration (often a saturated or near-saturated monovalent salt). In all DNA biosensor experiments, the biochemical hybridization reaction occurs in an electrolytic aqueous medium. The biological recognition will only proceed under specific conditions of ionic strength, solution's pH, and temperature. The molecular electrostatics and chemistry of the DNA molecule are very important in dictating the interaction of the DNA with its surroundings. Specificity is obtained by the unique affinity of binding between the probe and target.

12.1.5 Graphene-Based Field Effect Transistors

GFETs as breakthrough results were reported by Manchester Group in 2004 [36]. Since that time, large numbers of attempts have also been made to use graphene as a novel channel material in FETs for electronics [37–42]. As shown in Figure 12.4, GFET structure consists of a 300-nm SiO_2 layer as a

back-gate dielectric and a doped silicon substrate as the back-gate has been proposed [43]. The graphene is sandwiched between the source and drain electrodes controlled by the gate through the gate voltage applied. The most interesting feature of graphene in transistors is providing the possibility of having channels that are just one atomic layer thick [22]. Plus the rewarding experiments on electronic, peripherals such as FET [44] made with the application of thin graphene plates [31] by nano-microlithographic fabrication [33]. This suggests and justifies the call for action and the necessity of further DNA detection studies [34] as well as understanding the high sensitivity of the transport carriers in graphene plates and the conductance response to environmental distress [35].

In the process of observing the conductance variations of fabricated device base carbon materials, electrical and label-free DNA detection hybridization was possible to attain [1]. Graphene conductive characteristic as a channel in the FETs was considered as a seminal electronic features in the material [45]. Presently, the attention has moved toward been a focus on the exploratory capabilities in single-layer graphene [46]. Besides, single-electron transistor base on monolayer graphene was discovered in an experiment as well [47]. Among the bonuses in the incorporation of graphene as an FETs' channel material is a great electrostatics control capability. Therefore, the reduction of short channel effect is anticipated [48].

12.1.6 DNA Sensor Structure

As shown in Figure 12.4, large graphene film has incorporated to be DNA detection template constructed of multi-layer and single-layer graphene with a ratio of 40 to 60 percent. These graphene films are made using the chemical vapor deposition (CVD) method [4, 49]. As a notable fact, transference of the graphene film from nickel to glass substrate results in the possibility of the fabrication of FET transistor based on large graphene [50]. The result of producing a DNA detection solution chamber was achieved through incorporating silver paint as source and drain electrodes and polydimethylsiloxanes (PDMS) as an insulator. The conductance between source and drain varies in response to the surface electric potential of graphene, and the gate electrode coupled through the liquid electrolytes is used to control the on and off switching of the devices. The configuration of the liquid-gated FETs (LGFETs) is possible with the incorporation of graphene films (Figure 12.4) which have the DNA molecule detection sensitivity of 0.01nM [51]. Another one of the abilities in this device is the detection of target DNA hybridization to the probe DNAs that are pre-fixated on graphene. Plus, it has the capability of differentiating

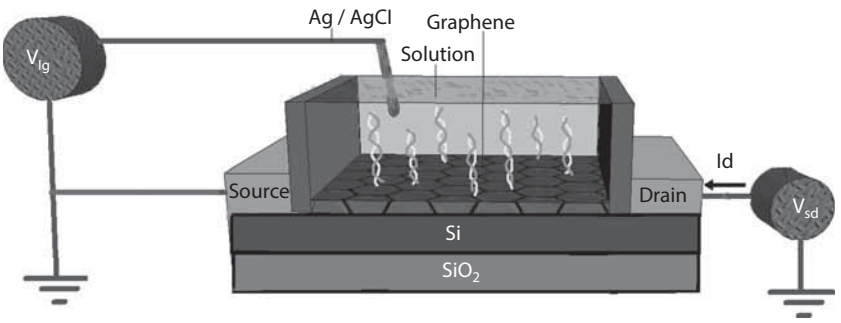

Figure 12.4 Proposed structure of graphene-based DNA sensor with liquid gate for DNA sensing

single-based incompatibility. Additionally, the harmonious DNA and the one-base incompatible DNA can be simply distinguished considering that $V_{g,min}$ is less sensitive to the incompatible DNA, which was responsible for 20 meV alteration at a high concentration (500 nM).

Ag/AgCl is used as a reference electrode in this experiment. The most significant reaction which plays a crucial role in determining the potential of the solution is the electron transfer reaction for electrodes. Three types of electrodes from electrochemical point are defined as: ideally polarizable, non-polarizable, and partially polarizable. This categorization differentiates electrode boundaries in terms of their capability to carry out current. A non-polarizable electrode is one which can freely allow electron transfer reactions without any hindrance. It is noteworthy that typically a reference electrode is anticipated to be non-polarizable; if not it could weaken the sensitivity of the biosensor. The reference electrode sets the potential of the solution by achieving electrochemical equilibrium with the solution via electron transfer reactions.

12.1.7 Sensing Mechanism

The (π–π) reactions among the carbon plane and the DNA molecules strongly affect the device conductivity of device by the means of different mechanisms like electronic doping [1] and electrostatic gating [2, 52]. Both the DNA and graphene are negative in charges; hence, the considerable role of buffer in ssDNA hybridizing sensing of graphene [53] is significant. Phosphate buffer saline (PBS) or sodium chloride solution has recurrently been incorporated in the form of a buffer for charge screening [54, 55]. The outcome of which is DNA adsorption due to both van Der Waals and electrical attraction [55, 56]. Meaning, the detection process could be defined as a transference of the electron between DNA and graphene films [5].

Built on the detection process, a DNA hybridization kinetic model was suggested with kinetic coefficients for surface-bound DNA probes [57]. Here in this research, the concentration of DNA in the form of a gate voltage is replicated and DNA sensing factor (α) is suggested. Eventually, the collation study between suggested model, and the data attained from the experiments are reported.

12.2 Numerical Modeling

Modeling and simulation incorporating partial differential equations (PDE) are an essential factor in the process of current–voltage characteristics, sensitivity, and the performance of the sensory peripherals that DNA molecules are exposed to. The proposed model here possesses the electrical detection of DNA hybridization performance capability by the means of simulating the conductance of the graphene plates. Built on the sensing process derived from the experiment to study the factors at lay in the absorption of DNA in relation to graphene, the function of gate voltage is presumed to be the DNA concentration with the implication of sensing factor (α). In this study, the selection of conductance in the form of a calculable sensory factor has taken place based on the fact of graphene nanomaterial's sensitivity to the presence of DNA molecules. Also, it can be argued that that the initiation of modeling from graphene conductance is valid.

12.2.1 Modeling of the Sensing Parameter (Conductance)

The conductivity of the graphene might show a discrepancy due to the variations of carrier density, carrier concentration, type of electron scattering at the edges, Fermi level, and chirality width [58]. Naeemi and Meindl [25] suggested that each conduction channel in graphene contributes one quantum. A district of the lowest G regards to gate voltage as a basic constant proportional to Planck's constant and electron charge in bulk graphene is defined and calculates for the minimum conductivity by the

$$G_0 = \frac{2e^2}{h} \tag{12.1}$$

Two factors make possible the conductance output in large channels, resulting in the capability of adhering to the Ohmic scaling law built upon the Landauer formula. The first is the self-sufficiency of the interface resistance length. The second would be a result of the nonlinearity relation

between the conductance and width that does rely on the quantity of modes in the conductor. Hence, the Landauer formula conductance would extend as the form of Equation (12.2) at the same time as these quantized parameters are taken into consideration.

$$G = \frac{2q2}{h}\int_{0}^{+\infty} M(E)T(E)\left(-\frac{df(E)}{dE}\right)dE \tag{12.2}$$

where q is the electron charge, h is Planck's constant, E is the energy band structure, $T(E)$ is the transmission probability, $M(E)$ is the number of modes at an applied energy near the wave vector which is dependent on the sub band's position, and $f(E)$ is the Fermi–Dirac distribution function. Without scattering, electrons in ballistic transport behave according to second law of Newton for motion of particle at non-relativistic speeds; so, the electrical resistivity can be neglected in a ballistic channel of graphene due to lack of scattering for electron transport [46, 59]. So, T would be defined as the probability of one injected electron at one end that can be transmitted to other end is considered equal to one ($T(E)$ =1) [60]. Additionally, $f(E)$ is the likelihood of the Fermi level, occupation with electrons that is defined as the Fermi–Dirac distribution function [61–63].

$$f(E) = \frac{1}{e^{\frac{E-EF}{k_B T}} + 1} \tag{12.3}$$

where E_F is the Fermi energy, k_B is the Boltzmann constant, and T is temperature. By applying the Maxwell–Boltzmann approximation, the distribution function can be expressed as

$$f(E) \approx \frac{1}{e^{\frac{E-E_F}{k_B T}}} = e^{-\frac{E-E_F}{k_B T}} \tag{12.4}$$

The graphene length has a seminal part in the definition of conductivity equation [64]. By the substitution of sub-bands (mode numbers) quantity in addition to the Fermi–Dirac distribution function in Equation (12.2), it is possible to obtain conductance as

$$G = \frac{3q^2}{h}\cdot\frac{a_{CC}t}{L}\cdot(3a_{CC}t)^{\frac{1}{2}}\cdot\left(\int_{0}^{+\infty}\left(E-\frac{2\beta 2}{3a_{CC}t}\right)^{\frac{1}{2}}\cdot d\left(-\frac{1}{1+e^{(E-E_F)/K_B T}}\right)\right) \tag{12.5}$$

By making the substitution of $x = (E–E_g)/K_BT$, the boundary of integral changes as follows. Equation (12.5) becomes

$$G = \frac{3q^2}{hL}\left(3\pi a_{CC}{}^3 t^3 K_B T\right)^{\frac{1}{2}} \cdot \left(\int_0^{+\infty} \frac{x^{\frac{1}{2}}}{\left(1+e^{x-\eta}\right)} dx + \int_0^{+\infty} \frac{x^{-\frac{1}{2}}}{\left(1+e^{x+\eta}\right)} dx \right) \tag{12.6}$$

where the normalized Fermi energy is defined as $\eta=(E_F–E_g)/K_BT$. The incorporation of the Fermi–Dirac integral (FDI) form of conductance will prove to be beneficial in order to comprehend the function of degenerate and non-degenerate regimes. It is noted that the FDI of an order *i* is defined as

$$\Im_i(\eta) = \frac{1}{\Gamma(i+1)} \int_0^{\infty} \frac{x^i}{1+e^{x-\eta}} dx \tag{12.7}$$

In general, $\Gamma(i+1) = \int_0^{\infty} e^{-x} x^i dx = i!$ if *i* is an integer applicable to gamma function, $\Gamma(1/2) = \sqrt{\pi}$ and $\Gamma(3/2) = (1/2)\,\Gamma(1/2) = \sqrt{\pi}/2$. A notable matter of observation is the common characteristics of the FDI in the non-degenerate and the heavily degenerate limits. Therefore, attaining the typical mode of graphene is similar to that of silicon as suggested by Gunlycke [65].

$$G = \frac{3q^2}{hL}\left(3\pi a_{CC}^3 t^3 K_B T\right)^{\frac{1}{2}} \left(\Im_{-\frac{1}{2}}(\eta) + \Im_{-\frac{1}{2}}(-\eta) \right) \tag{12.8}$$

where $\Im_{-\frac{1}{2}}(\eta)$is the FDI of order $(-\frac{1}{2})$. The distribution function of Fermi–Dirac is ascribed to degenerate and non-degenerate states with the quantity of *(η >> 0)* and (η ≪ 0) each. During the non-degenerate state, the approximation of FDI is possible using Maxwell–Boltzmann distribution factor of (E)=exp(η^{η}). Therefore, in the nondegenerate limit, graphene's general conductance model can be transformed into the exponential equation as [66, 67].

$$G = \frac{3q^2}{hL}\left(3\pi a_{CC}{}^3 t^3 K_B T\right)^{\frac{1}{2}} \left(e^{(\eta)} + e^{(-\eta)}\right) \tag{12.9}$$

As normalized Fermi energy derived as $\eta = (E–E_g)/K_BT$, and the band-gap energy is $E_g = q.v_g$; then, the normalized Fermi energy is calculated

as $\eta = (V_t - V_g)/K_B Tq$ which correspond to a function of V_g. Employing η in Equation (12.9), the conductance expresses as

$$G = \mp \frac{3q^2}{hL}\left(3a_{CC}{}^3 t^3 \pi K_B T\right)^{\frac{1}{2}}\left(e^{\left(V_t - V_g/K_B Tq\right)} + e^{\left(-V_t + V_g/K_B Tq\right)}\right) \tag{12.10}$$

which represents conductance (G) as a function of gate voltage (V_g). Figure 12.3 would display graphene-based DNA sensor conductance model in comparison to the gate voltage prior to the addition of a DNA molecule. Based on the data gathered from the experiment, the suggested model can meet the major expectation of graphene-based DNA sensor [1].

The simulation results demonstrated that the conductance in graphene is minimum at the Dirac point, suggesting that the resistance is higher at the point closest to the charge neutrality point.

12.2.2 Current–Voltage (I_d–V_g) Characteristics Modeling

The DNA sensor's performance built upon graphene nanostructure is assessed by the incorporation of its current–voltage properties [68]. Additionally, by replacing the FDI in Equation (12.10), the general conductance model of single-layer graphene would be obtained as

$$\mathrm{I_d} = \frac{3q^2\left(3\pi a^3 t^3 k_{BT}\right)^{\frac{1}{2}}}{hL}\left[\Im_{-\frac{1}{2}}(\eta) + \Im_{-\frac{1}{2}}(-\eta)\right]\left(V_{gs} - V_t\right) \tag{12.11}$$

where V_{gs} is the gate-source voltage, and V_t is the threshold voltage. As shown in Figure 12.4, prior to the addition of the probe DNA, pure PBS (40 μL) has been added to the chamber in order to calculate the transfer curve, in other words, drain current (I_d) in comparison to the gate voltage [51]. A valid consensus is observable among the suggested model for DNA sensor and the outcome of the experiments obtained from the reference [51].
Since the DNA molecules need to saturate the graphene surface, high concentration of probe DNAs (1 μM) in 40 μL PBS buffer has been added to the chamber. As seen in Figure 12.5, the application of the gate voltage to the DNA solution will result in (graphene-based FETs) clear display of the ambipolar conductance behavior. The doping states of graphene have been controlled by the $V_{g,min}$ to calculate the graphene plate's lowest level of conductance as determined by transfer characteristic curve.

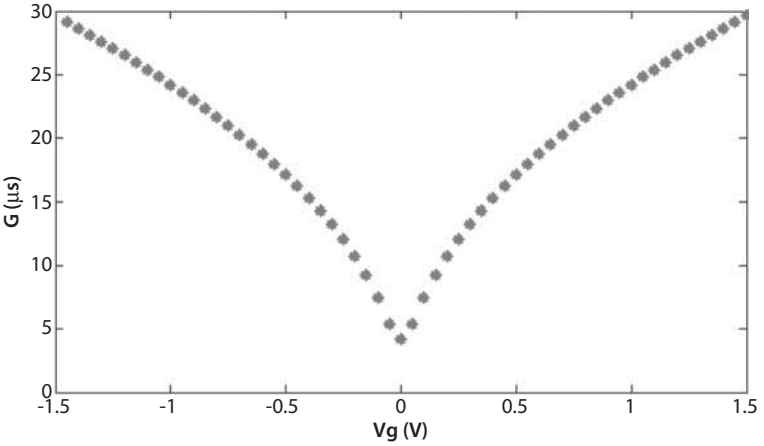

Figure 12.5 Conductance model of graphene-based LGFETs prior to addition of DNA molecules.

12.2.3 Proposed Alpha Model

The considerable left shift of $V_{g,min}$ is a result of the fixation of probe DNA upon on the graphene surface, then is dramatically left shifted. Based on this, it is reasonable to conclude that $V_{g,min}$ is greatly sensitive to the probe DNA and hybridization and fixation of harmonious target DNAs. In order to support this conclusion, the observation of gate voltage change toward left as a result of DNA molecules doping the graphene film is helpful [3, 69]. However, the increased number of carriers affects the conductivity of the (graphene) FET devices in the channel. The attachment among graphene and nucleotides was experimented and researched [42, 69, 70]. Commonly, $V_{g,min}$ turn is to be considered as a legitimate hint toward DNA detection. Ultimately, the harmonious DNAs with concentration of 40 **μL** were appended to the device made for hybridization using probe-DNA-fixated graphene [51]. It can be seen in Figure 12.6 that, during the expansion of concentrated harmonious DNAs from 0.01 to 500 nM, additional DNA molecules will be adsorbed and the attraction of additional molecules would be possible, resulting in alteration of $V_{g,min}$ on the properties which relies on and will calculate the location of the Fermi level respective to the conduction band border.

Inspired by this fact, the gate voltage is simulated as a function of DNA concentration and DNA immobilization factor (α) is recommended. Eventually, the variation in the gate voltage can be modeled by DNA

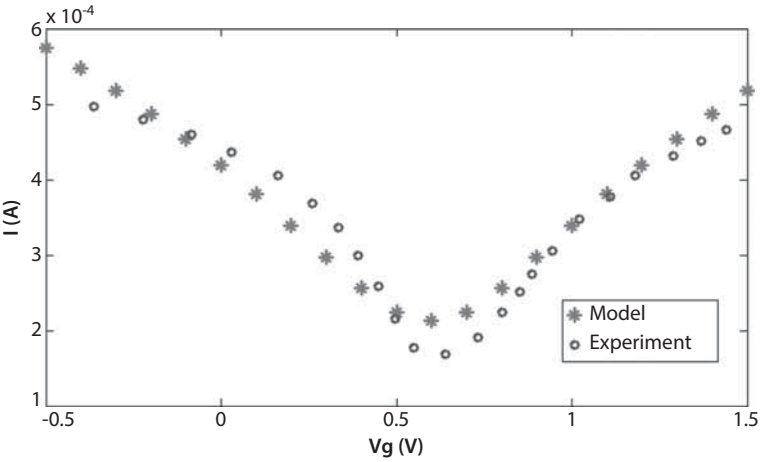

Figure 12.6 Comparison of the proposed numerical model (starred line) with experiment (circle line) for bare sensor.

concentration factor (F), i.e., V_g after hybridization is assumed as a function of DNA concentration and gate voltage without DNA molecules, as follows:

$$V_{gs(DNA)} = \frac{a(F)}{1} V_{gs(withoutDNA)} \tag{12.12}$$

In the nonsaturation region, the DNA concentration model is employed as a function of gate voltage, and the ideal current–voltage relation for the n-channel FET from Equations (12.11 and 12.12) is customized as

$$I_d = \frac{3q^2\left(3\pi a^3 t^3 k_{BT}\right)^{\frac{1}{2}}}{hL}\left[\Im_{-\frac{1}{2}}(\eta) + \Im_{-\frac{1}{2}}(-\eta)\right]\left(aV_{gs(withoutDNA)} - V_t\right) \tag{12.13}$$

where q is the electron charge, a = 1.42 Å defines carbon–carbon (C–C) bond length, t=2.7 (eV)is the nearest neighbor C–C tight binding overlap energy, K_B is the Boltzmann's constant, T represents temperature, h is Planck's constant, and L denotes the length of conducting channel. V_{gs} presents the gate-source voltage, and refers to the threshold voltage. Furthermore, $\Im_{-\frac{1}{2}}(\eta)$, and $\Im_{-\frac{1}{2}}(-\eta)$ are the FDIs of orders $-\frac{1}{2}$, which can be solved numerically. Its value depends on which measures the location of the Fermi level with respect to the conduction band edge. The Fermi–Dirac

distribution function has divergent manifestations in degenerate and non-degenerate states which are ascribed to ($\eta >> 0$) each.

In order to validate this hypothesis, the models of I_d–V_g properties of LGFET for DNA concentration altering from 0.01 to 500 nM are represented. The Fermi–Dirac distribution function has different forms in degenerate and non-degenerate states which are attributed by (η>>0), respectively [71, 72]. α is a DNA immobilization factor, and different concentrations of DNA molecules are presented in the form of *F* parameter. Thus, the DNA molecules are adsorbed on graphene surface by iteration method was modeled as

$$\alpha = \left(\mathrm{aF}^2 + \mathrm{bF} + \mathrm{c}\right) / F \tag{12.14}$$

A=13, *B*=50, and *C*=4070parameters are calculated based on iteration method. The current–voltage characteristic of LGFET according to the proposed model of DNA sensor using nanostructured graphene layer is obtained as

$$\mathrm{I_d} = \frac{3q^2\left(3\pi a^3 t^3 k_{BT}\right)^{\frac{1}{2}}}{hL}\left[\Im_{-\frac{1}{2}}(\eta) + \Im_{-\frac{1}{2}}(-\eta)\right]\left(\frac{13\mathrm{F}^2 + 50\mathrm{F} + 4070}{F}V_{gs(withoutDNA)} - V_t\right) \tag{12.15}$$

As discussed here, the drain source current of the LGFET as a function of gate voltage is simulated; moreover, DNA immobilization factor as a function of DNA concentration factor (*F*) is suggested. In order to

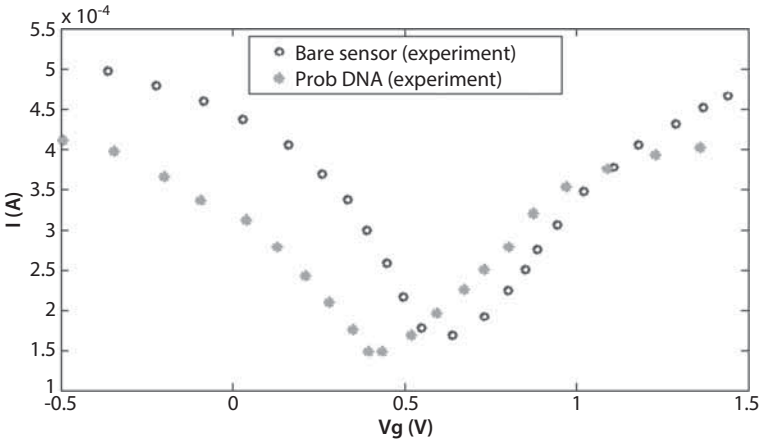

Figure 12.7 The current–voltage characteristic of graphene-based FET with the presence of probe DNAs (1 μM).

validate this hypothesis, the models of I_d–V_g properties of LGFET for DNA concentration altering from 0.01 to 500 nM are represented in Figure 12.7. The comparison of the experiment outcome with the theoretical modeling [73], it would be a legitimate statement that the sensor model based on the proposed parameters stipulates the directions that have been outlined by the data gathered from the experiments.

12.2.4 Comparison of the Proposed Numerical Model with Experiment

As shown in Figure 12.7, the suggested model indicates the cogent concentration reliance on current–voltage property, displaying the influence of the concentration increment effect on the minimum voltage conductance. Meaning that, the $V_{g,min}$, as mentioned in the data gathered from the experiments, will be moved towards left and the quantity of movement escalates with the growing concentration of the harmonious DNA from 0.01 to 10 nM as stated by experimental results [73]. Figures 12.8 and 12.9 describe the I_d–V_g characteristic of the proposed numerical model with the experimental data for different concentrations of complementary DNA. As shown in Fig. 8a–c that each diagram depicts specific concentration of DNA molecules as F=0.01 nM, F=0.1 nM, and F=10 nM, respectively.

Another observation made in the experiment is that, the variation of, I_d–V_g property is a result of DNA concentration made possible by the DNA immobilization factor (Figure 12.10). Furthermore, the proposed model presents strongly approximate results compared with experimental data. According to Figure 12.9a and b, the amount of $V_{g,min}$ shift remains unchanged by increasing the DNA concentration from 10 to 500nM, holding the fact that the number of DNA molecules is limited and the graphene surface has become saturated. The electron transfer from DNA molecules (electron rich) to graphene have been explored experimentally in Ref. [51]. Also, as shown in Figure 12.9a and b, each diagram depicts specific concentration of DNA molecules. For example, when concentration value is F=100 nM, the model is closer to the blue line; in the same manner we can compare other concentrations as well (Figure12.11).

The proposed numerical model with coupled with experimental data is shown in this work to confirm that the conductivity of the graphene-based DNA sensor is decreased by the introduction of DNA molecules.

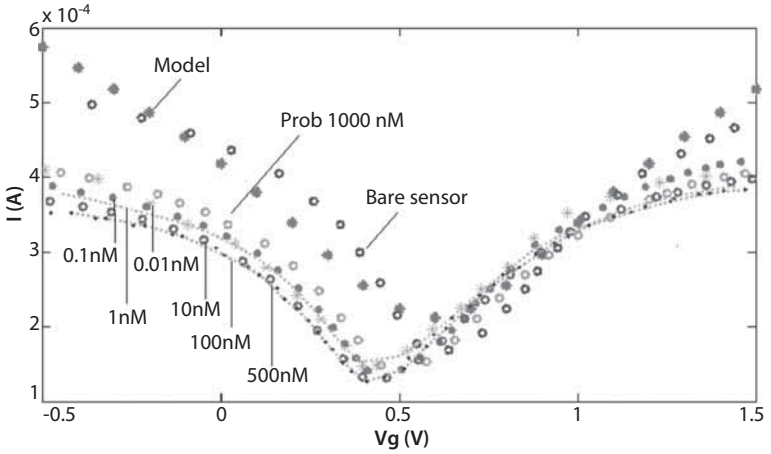

Figure 12.8 The current–voltage characteristic of LGFET applied to different concentration of DNA molecules (0.01–500 nM).

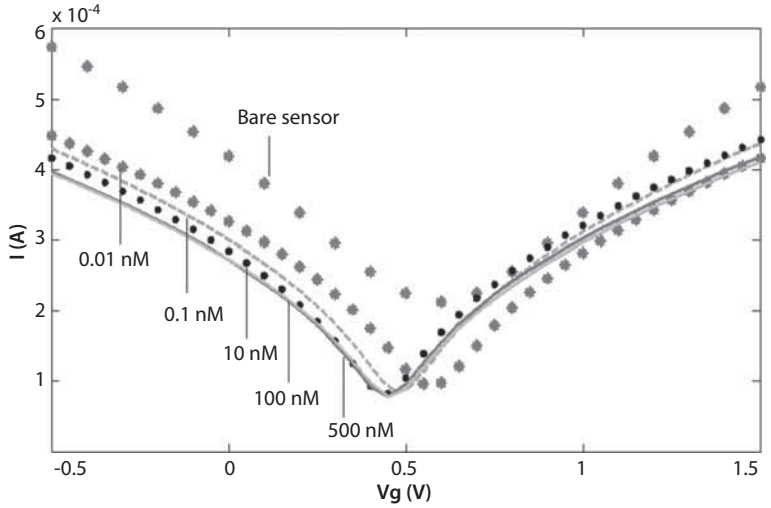

Figure 12.9 All numerical models of I_d–V_g characteristics altering from 0.01 to 500 nM.

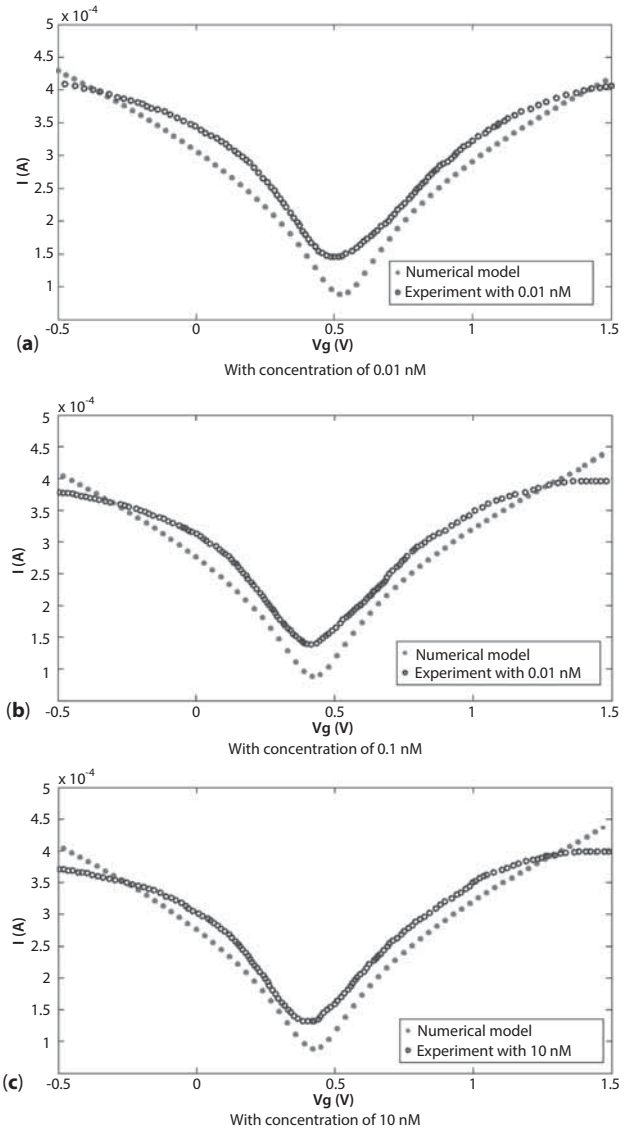

Figure 12.10 The I_d–V_g characteristic of the proposed alpha model comparing with the extracted experimental data for the specific DNA concentration of (a) F=0. 01 nM, (b) F=0. 1 nM, and (c) F=10 nM.

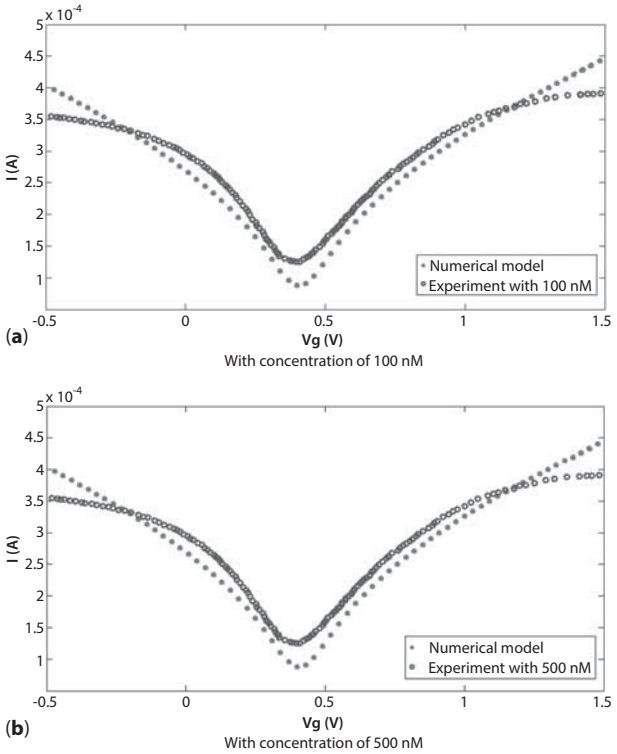

Figure 12.11 The I_d–V_g characteristics of the proposed alpha model with the experimental data for DNA concentration of (a) F=100 nM and (b) F=500 nM.

References

1. A. Star, *et al.*, "Label-free detection of DNA hybridization using carbon nanotube network field-effect transistors," *Proceedings of the National Academy of Sciences of the United States of America,* vol. 103, p. 921, 2006.
2. D. Fu and L. J. Li, "Label-free electrical detection of DNA hybridization using carbon nanotubes and graphene," *Nano Reviews,* vol. 1, 2010.
3. N. Mohanty and V. Berry, "Graphene-based single-bacterium resolution biodevice and DNA transistor: interfacing graphene derivatives with nanoscale and microscale biocomponents," *Nano Letters,* vol. 8, pp. 4469–4476, 2008.
4. A. Reina, *et al.*, "Large area, few-layer graphene films on arbitrary substrates by chemical vapor deposition," *Nano Letters,* vol. 9, pp. 30–35, 2008.

5. Y. Wen, *et al.*, "A graphene-based fluorescent nanoprobe for silver (I) ions detection by using graphene oxide and a silver-specific oligonucleotide," *Chemical Communications,* vol. 46, pp. 2596–2598, 2010.
6. K. S. Novoselov, *et al.*, "Electric field effect in atomically thin carbon films," *Science,* vol. 306, pp. 666–669, 2004.
7. K. S. Novoselov, *et al.*, "Two-dimensional atomic crystals," *Proceedings of the National Academy of Sciences of the United States of America,* vol. 102, pp. 10451–10453, 2005.
8. R. Grassi, *et al.*, "Graphene nanoribbons FETs for high-performance logic applications: perspectives and challenges," *9th International Conference on Solid-State and Integrated-Circuit Technology,* vol. 1, pp. 365–368, 2008.
9. G. C. Liang, *et al.*, "Performance projections for ballistic graphene nanoribbon field-effect transistors," *IEEE Transactions on Electron Devices,* vol. 54, pp. 677–682, 2007.
10. K. I. Bolotin, *et al.*, "Ultrahigh electron mobility in suspended graphene," *Solid State Communications* vol. 146, pp. 351–355, 2008.
11. K. S. Novoselov, *et al.*, "Electric field effect in atomically thin carbon films," *Science,* vol. 306, pp. 666–669, 2004.
12. F. Schedin, *et al.*, "Detection of individual gas molecules adsorbed on graphene," *Nature Materials,* vol. 6, pp. 652–655, 2007.
13. K. Welsher, *et al.*, "Selective probing and imaging of cells with single walled carbon nanotubes as near-infrared fluorescent molecules," *Nano Letters,* vol. 8, pp. 586–590, 2008.
14. Y. Shi, *et al.*, "Effective doping of single-layer graphene from underlying SiO_2 substrates," *Physical Review B,* vol. 79, p. 115402, 2009.
15. J. Kong, *et al.*, "Nanotube molecular wires as chemical sensors," *Science,* vol. 287, p. 622, 2000.
16. P. G. Collins, *et al.*, "Extreme oxygen sensitivity of electronic properties of carbon nanotubes," *Science,* vol. 287, p. 1801, 2000.
17. E. Snow, *et al.*, "Chemical detection with a single-walled carbon nanotube capacitor," *Science,* vol. 307, p. 1942, 2005.
18. Y. B. Shi, *et al.*, "Binary channel SAW mustard gas sensor based on PdPc(0.3) PANI(0.7)hybrid sensitive film," in *4th International Symposium on Instrumentation Science and Technology*. vol. 48, J. Tan, ed., 2006, pp. 292–297.
19. T. Wehling, *et al.*, "Molecular doping of graphene," *Nano Letters,* vol. 8, pp. 173–177, 2008.
20. X. Dong, *et al.*, "Doping single-layer graphene with aromatic molecules," *Small,* vol. 5, pp. 1422–1426, 2009.
21. M. Zheng, *et al.*, "DNA-assisted dispersion and separation of carbon nanotubes," *Nature Material,* vol. 2, pp. 338–342, 2003.
22. F. Schwierz, "Graphene transistors," *Nature Nanotechnology,* vol. 5, pp. 487–496, 2010.
23. Y.-J. Kang, *et al.*, "Electronic structure of graphene and doping effect on SiO_2," *Physical Review B,* vol. 78, p. 115404, 2008.

24. Y.-W. Son, *et al.*, "Energy Gaps in Graphene Nanoribbons," *Physical Review Letters,* vol. 97, p. 216803, 2006.
25. W. Zhang, *et al.*, "Opening an electrical band gap of bilayer graphene with molecular doping," *ACS Nano,* vol. 5, pp. 7517–7524, 2011.
26. Y. Zhang, *et al.*, "Direct observation of a widely tunable bandgap in bilayer graphene," *Nature,* vol. 459, pp. 820–823, 2009.
27. V. Ryzhii, *et al.*, "Device model for graphene bilayer field-effect transistor," *Journal of Applied Physics,* vol. 105, p. 4510, 2009.
28. Y. Ouyang, *et al.*, "Analysis of ballistic monolayer and bilayer graphene field-effect transistors," *Applied Physics Letters,* vol. 92, p. 063120, 2008.
29. C. Mastrangelo, "DNA analysis systems on a chip," *Advances in Science and Technology,* vol. 26, pp. 465–476, 1999.
30. M. W. Shinwari, "Static and dynamic modeling of DNA biosensors for biomedical applications," 2011.
31. K. S. Novoselov, *et al.*, "Two-dimensional gas of massless Dirac fermions in graphene," *Nature,* vol. 438, pp. 197–200, 2005.
32. N. Varghese, *et al.*, "Binding of DNA nucleobases and nucleosides with graphene," *Chemphyschem,* vol. 10, pp. 206–210, 2009.
33. L. X. Dong and Q. Chen, "Properties, synthesis, and characterization of graphene," *Frontiers of Materials Science in China,* vol. 4, pp. 45–51, 2010.
34. T. G. Drummond, *et al.*, "Electrochemical DNA sensors," *Nature biotechnology,* vol. 21, pp. 1192–1199, 2003.
35. Y. Huang, *et al.*, "Graphene-based biosensors for detection of bacteria and their metabolic activities," *Journal of Materials Chemistry,* vol. 21, pp. 12358–12362, 2011.
36. K. Novoselov, *et al.*, "Electric field effect in atomically thin carbon films," *Science,* vol. 306, p. 666, 2004.
37. F. Karimi, *et al.*, "Analytical modeling of graphene-based DNA sensor," *Science of Advanced Materials,* vol. 4, pp. 1142–1147, 2012.
38. K. Xu, *et al.*, "Graphene-based FET structure: modeling FET characteristics for an aptamer-based analyte sensor," in *Computational Electronics (IWCE), 2012 15th International Workshop on*, 2012, pp. 1–4.
39. D. Chen, *et al.*, "Graphene-based materials in electrochemistry," *Chemical Society Reviews,* vol. 39, pp. 3157–3180, 2010.
40. H. K. F. Abadi, *et al.*, "Semi analytical modeling of quantum capacitance of graphene-based ion sensitive field effect transistor," *Journal of Computational and Theoretical Nanoscience,* vol. 11, pp. 596–600, 2014.
41. H. Karimi, *et al.*, "Analytical prediction of liquid-gated graphene nanoscroll biosensor performance," *RSC Advances,* vol. 4, pp. 16153–16162, 2014.
42. L.-J. Wang, *et al.*, "A graphene quantum dot with a single electron transistor as an integrated charge sensor," *Applied Physics Letters,* vol. 97, 2010.
43. X. Dong, *et al.*, "Synthesis and application of graphene nanoribbons," *Current Physical Chemistry,* vol. 3, pp. 291–301, 2013.

44. J. Nilsson, *et al.*, "Transmission through a biased graphene bilayer barrier," *Physical Review B (Condensed Matter and Materials Physics),* vol. 76, pp. 165416-10, 2007.
45. M. Dankerl, *et al.*, "Graphene solution-gated field-effect transistor array for sensing applications," *Advanced Functional Materials,* vol. 20, pp. 3117–3124, 2010.
46. D. S. L. Abergel, *et al.*, "Properties of graphene: a theoretical perspective," *Advances in Physics,* vol. 59, pp. 261–482, 2010.
47. T. Cohen-Karni, *et al.*, "Graphene and nanowire transistors for cellular interfaces and electrical recording," *Nano Letters,* vol. 10, pp. 1098–1102, 2010.
48. J. Choi, *et al.*, "Graphene used for device and graphene sheet, comprises etched edge portion comprising functional group of carbonyl, carboxy, hydroxy, formyl and/or oxycarbonyl," US2010178464-A1; KR2010083954-A.
49. A. Reina, *et al.*, "Growth of large-area single-and bi-layer graphene by controlled carbon precipitation on polycrystalline Ni surfaces," *Nano Research,* vol. 2, pp. 509-516, 2009.
50. C.-A. Di, *et al.*, "Interface engineering: an effective approach toward high-performance organic field-effect transistors," *Accounts of Chemical Research,* vol. 42, pp. 1573–1583, 2009.
51. X. Dong, *et al.*, "Electrical detection of DNA hybridization with single-base specificity using transistors based on CVD-grown graphene sheets," *Advanced Materials,* vol. 22, pp. 1649, 2010.
52. A. T. Johnson Jr, *et al.*, "Single walled carbon nanotubes functionally adsorbed to biopolymers for use as chemical sensors," ed: Google Patents, 2011.
53. R. Tel-Vered, *et al.*, "Biohybrid electrochemical devices," *Electrochemistry of Functional Supramolecular Systems,* vol. 6, p. 333, 2010.
54. J. H. Chen, *et al.*, "Charged-impurity scattering in graphene," *Nature Physics,* vol. 4, pp. 377–381, 2008.
55. X. Dong, *et al.*, "Electrical detection of DNA hybridization with single-base specificity using transistors based on CVD-grown graphene sheets," *Advanced Materials,* vol. 22, pp. 1649–1653, 2010.
56. W. Wang and S. He, "Theoretical analysis on response mechanism of polymer-coated chemical sensor based Love wave in viscoelastic media," *Sensors and Actuators B-Chemical,* vol. 138, pp. 432–440, 2009.
57. D. Erickson, *et al.*, "Modeling of DNA hybridization kinetics for spatially resolved biochips," *Analytical Biochemistry,* vol. 317, pp. 186–200, 2003.
58. Y. Wu and P. A. Childs, "Conductance of graphene nanoribbon junctions and the tight binding model," *Nanoscale Research Letters,* vol. 6, 2011.
59. A. F. Avila, *et al.*, "Hybrid nanocomposites for mid-range ballistic protection," *International Journal of Impact Engineering,* vol. 38, pp. 669–676, 2011.
60. S. Datta, *Electronic Transport in Mesoscopic Systems*. Cambridge, UK: Cambridge University Press, 2002.

61. B. Polash and H. F. Huq, "Analytical model of carbon nanotube field effect transistors for NEMS applications," *2008 51st Midwest Symposium on Circuits and Systems,* Vols. 1 and 2, pp. 61–64, 2008.
62. M. T. Ahmadi, *et al.*, "Numerical study of Fermi energy for P-type silicon nanowire," *Nanoscience and Nanotechnology,* vol. 1136, pp. 98–102, 2009.
63. J. Karamdel, *et al.*, "Formulation and simulation for electrical properties of a (5,3) single wall carbon nanotube," *ICSE: 2008 IEEE International Conference on Semiconductor Electronics, Proceedings,* pp. 545–548, 2008.
64. N. Peres, *et al.*, "Conductance quantization in mesoscopic graphene," *Physical Review B,* vol. 73, p. 195411, 2006.
65. D. Gunlycke, *et al.*, "Semiconducting graphene nanostrips with edge disorder," *Applied Physics Letters,* vol. 90, p. 142104, 2007.
66. R. B. Dingle and R. Dingle, *Asymptotic expansions: their derivation and interpretation*. London: Academic Press, 1973.
67. J. Zaharah, *et al.*, "Modelling of graphene nanoribbon Fermi energy," *Journal of Nanomaterials,* vol. 2010, 2010.
68. M. Passlack, "III-V Metal-oxide-semiconductor technology," *2008 IEEE 20th International Conference on Indium Phosphide and Related Materials (IPRM),* pp. 59–59, 2008.
69. Z. Liu, *et al.*, "PEGylated nanographene oxide for delivery of water-insoluble cancer drugs," *Journal of the American Chemical Society,* vol. 130, pp. 10876–10877, 2008.
70. S. Manohar, *et al.*, "Peeling single-stranded DNA from graphite surface to determine oligonucleotide binding energy by force spectroscopy," *Nano Letters,* vol. 8, pp. 4365–4372, 2008.
71. M. J. Kiani, *et al.*, "Analytical modelling of monolayer graphene-based ion-sensitive FET to pH changes," *Nanoscale Research Letters,* vol. 8, pp. 1–9, 2013.
72. H. K. F. Abadi, *et al.*, "Current–voltage modeling of graphene-based DNA sensor," *Neural Computing and Applications,* pp. 1–5, 2013.
73. N. Varghese, *et al.*, "Binding of DNA nucleobases and nucleosides with graphene," *ChemPhysChem,* vol. 10, pp. 206–210, 2009.